

An Empirical Analysis of Image-Based Learning Techniques for Malware Classification

Pratikkumar Prajapati* Mark Stamp†,§

Abstract

In this paper, we consider malware classification using deep learning techniques and image-based features. We employ a wide variety of deep learning techniques, including multilayer perceptrons (MLP), convolutional neural networks (CNN), long short-term memory (LSTM), and gated recurrent units (GRU). Amongst our CNN experiments, transfer learning plays a prominent role—specifically, we test the VGG-19 and ResNet152 models. As compared to previous work, the results presented in this paper are based on a larger and more diverse malware dataset, we consider a wider array of features, and we experiment with a much greater variety of learning techniques. Consequently, our results are the most comprehensive and complete that have yet been published.

1 Introduction

Traditionally, malware detection and classification has relied on pattern matching against signatures extracted from specific malware samples. While simple and efficient, signature scanning is easily defeated by a number of well-known evasive strategies. This fact has given rise to statistical and machine learning based techniques, which are more robust to code modification. In response, malware writers have developed advanced forms of malware that alter statistical and structural properties of their code, which can cause statistical models to fail.

In this paper, we compare deep learning (DL) models for malware classification. For most of our deep learning models, we use image-based features, but we also experiment with opcode features. The DL models consider include a wide variety of neural networking techniques, including multilayer perceptrons (MLP), several variants of convolutional neural networks (CNN), and vanilla recurrent neural networks (RNN), as well as the advanced RNN architectures known as long short-term memory (LSTM) and gated recurrent units (GRU). We also experiment with a complex stacked model that combines both LSTM and GRU. In addition, we consider transfer learning, in the form of the ResNet152 and VGG-19 architectures.

The remainder of this paper is organized as follows. In Section 2 we provide relevant background information, including a discussion of related work, an overview of the various learning techniques considered, and we introduce the dataset used in this research. Section 3 is the heart of the paper, with detailed results from a wide variety of malware classification experiments. Section 4 concludes the paper and provides possible directions for future work.

2 Background

In this section, we discuss related work and we introduce the various learning techniques that are considered in this research. We also discuss the dataset that we use in our malware classification experiments. In addition, we provide the specifications of the hardware and software that we use to conduct the extensive set of experiments that are summarized in Section 3.

2.1 Related Work

To the best of our knowledge, image-based analysis was first applied to the malware problem in [16], where high-level “gist” descriptors are used as features. More recently, [44] confirmed the results in [16] and presented an alternative deep learning approach that produces equally good—if not slightly better—results, without the extra work required to extract gist descriptors.

Transfer learning, where the output layer of an existing pre-trained DL model is retrained for a specific task, is often used in image analysis. Such an approach allows for efficient training, as a new model can take advantage of a vast amount of learning that is embedded in the pre-trained model.

*pratikkumar.prajapati@sjsu.edu

†mark.stamp@sjsu.edu

§Department of Computer Science, San Jose State University, San Jose, California

Leveraging the power of transfer learning has been shown to yield strong image-based malware detection and classification results [44].

There is a vast malware analysis literature involving classic machine learning techniques. Representative examples include [2], [5], [8], [25], [28], [42]. Intuitively, we might expect models based on image analysis to be somewhat stronger and more robust, as compared to models that rely on opcodes, byte n -grams, or similar statistical features that are commonly used in malware research.

The work presented in this paper can be considered an extension of the work in [6], where image-based transfer learning is applied to the malware classification problem. We have extended this previous work in multiple dimensions, including a larger, more challenging, and more realistic dataset. In addition, we perform much more experimentation with a much wider variety of techniques, and we consider a large range of hyperparameters in each case.

2.2 Learning Techniques

In this section, we provide a brief introduction to each of the learning techniques considered in this paper. Additional details on most of the learning techniques discussed here can be found in [27], which includes examples of relevant applications of the techniques. We provide additional references for the techniques discussed below that are not considered in [27].

2.2.1 Multilayer Perceptron

A perceptron computes a weighted sum of its components in the form of a hyperplane, and based on a threshold, a perceptron can be used to define a classifier. It follows that a perceptron cannot provide ideal separation in cases where the data itself is not linearly separable. This is a severe limitation, as something as elementary as the XOR function is not linearly separable.

A multilayer perceptron (MLP) is an artificial neural network that includes multiple (hidden) layers in the form of perceptrons. Unlike a single layer perceptron, MLPs are not restricted to linear decision boundaries, and hence an MLP can accurately model more complex functions. The relationship between perceptrons and MLPs is very much analogous to the relationship between linear support vector machines (SVM) and SVMs based on nonlinear kernel functions.

Training an MLP would appear to be challenging since we have hidden layers between the input and output, and it is not clear how changes to the weights in these hidden layers will affect each other or the output. Today, MLPs are generally trained using backpropagation. The discovery that backpropagation can be used for training neural networks was a major breakthrough that made deep learning practical.

2.2.2 Convolutional Neural Network

Generically, artificial neural networks use fully connected layers. The advantage of a fully connected layer is that it can deal effectively with correlations between any points within training vectors. However, for large training vectors, fully connected layers are infeasible, due to the vast number of weights that must be learned.

In contrast, a convolutional neural network (CNN), is designed to deal with local structure. A convolutional layer cannot be expected to perform well when significant information is not local. The benefit of CNNs is that convolutional layers can be trained much more efficiently than fully connected layers, due to the reduced number of weights.

For images, most of the important structure (edges and gradients, for example) is local. Hence, CNNs are an ideal tool for image analysis and, in fact, CNNs were developed precisely for image classification. However, CNNs have performed well in a variety of other problem domains. In general, any problem for which local structure predominates is a candidate for CNNs.

2.2.3 Recurrent Neural Network

MLPs and CNNs are feedforward neural networks, that is, the data feeds directly through the network, with no “memory” of previous feature vectors. In a feedforward network, each input vector is treated independently of other input vectors. While feedforward networks are appropriate for many problems, they are not well-suited for dealing with sequential data.

In some cases, it is necessary for a classifier to have memory. Suppose that we want to tag parts of speech in English text (i.e., noun verb, etc.), this is not feasible if we only look at words in isolation. For example, the word “all” can be an adjective, adverb, noun, or pronoun, and this can only be determined by considering its context. A recurrent neural network (RNN) provides a way to add memory (or context) to a feedforward neural network.

RNNs are trained using a variant of backpropagation known as backpropagation through time (BPTT). A problem that is particularly acute in BPTT is that the gradient calculation tends to become unstable, resulting in “vanishing” or “exploding” gradients. To overcome these problems, we can limit the number of time steps, but this also serves to limit the utility of RNNs. Alternatively, we can use specialized RNN architectures that enable the gradient to flow over long time periods. Both long short-term memory and gated recurrent units are examples of such specialized RNN architectures. We discuss these two RNN architectures next.

2.2.4 Long Short-Term Memory

Long short-term memory (LSTM) networks are a class of RNN architectures that are designed to deal with long-range dependencies. That is, LSTM can deal with extended “gaps” between the appearance of a feature and the point at which it is needed by the model. In plain vanilla RNNs this is generally not possible, due vanishing gradients.

The key difference between an LSTM and a generic vanilla RNN is that an LSTM includes an additional path for information flow. That is, in addition to the the hidden state, there is a so-called cell state that can be used to, in effect, store information from previous steps. The cell state is designed to serve as a gradient “highway” during backpropagation. In this way, the gradient can “flow” much further back with less chance that it will vanish (or explode) along the way.

As an aside, we note that the LSTM architecture has been one of the most commercially successful learning techniques ever developed. Among many other applications, LSTMs play a critical role in Google Allo [11], Google Translate [43], Apple’s Siri [13], and Amazon Alexa [9].

2.2.5 Gated Recurrent Unit

Due to its wide success, many variants on the LSTM architecture have been considered. Most such variants are slight, with only minor changes from a standard LSTM. However, a gated recurrent unit (GRU) is a fairly radical departure from an LSTM. Although the internal state of a GRU is somewhat complex and less intuitive than that of an LSTM, there are fewer parameters in a GRU. As a result, it is easier to train a GRU than an LSTM, and consequently less training data is required.

2.2.6 ResNet152

Whereas LSTM uses a complex gating structure to ease gradient flow, a residual network (ResNet) defines additional connections that correspond to identity layers. These identity layers allow a ResNet model to, in effect, skip over layers during training, which serves to effectively reduce the depth when training and thereby mitigate gradient pathologies. Intuitively, ResNet is able to train deeper networks by training over a considerably shallower network in the initial stages, with later stages of training serving to flesh out the intermediate connections. This approach was inspired by pyramidal cells in the brain, which have a similar characteristic, in the sense that they bridge “layers” of neurons [26].

ResNet152 is a specific deep ResNet architecture that has been pre-trained on a vast image dataset. As one of our two examples of transfer learning, we use this architecture, which includes an astounding 152 layers. That is, we use the ResNet152 model, where we only retrain the output layer specifically for our malware classification problem.

2.2.7 VGG-19

VGG-19 is a 19-layer convolutional neural network that has been pre-trained on a dataset containing more than 10^6 images [24]. This architecture has performed well in many contests, and it has been generalized to a variety of image-based problems. Here, we use the VGG-19 architecture and pre-trained model as one of our two examples of transfer learning for image-based malware classification.

2.3 Dataset

Our dataset consists of 20 malware families. Three of these malware families, namely, Winwebsec, Zeroaccess, and Zbot, are from the Malicia dataset [15], while the remaining 17 families are taken from the massive malware dataset discussed in [12]. This latter dataset is almost half a terabyte and contains more than 500,000 malware samples in the form of labeled executable files.

Table 1 lists the 20 families used in this research, along with the type of malware present in each family. Next, we briefly discuss each of these 20 malware families.

Table 1: Type of each malware family

Family	Type	Family	Type
Adload [29]	Trojan Downloader	Obfuscator [37]	VirTool
Agent [30]	Trojan	Onlinegames [22]	Password Stealer
Alureon [35]	Trojan	Rbot [38]	Backdoor
BHO [32]	Trojan	Renos [31]	Trojan Downloader
CeeInject [34]	VirTool	Startpage [33]	Trojan
Cycbot [3]	Backdoor	Vobfus [39]	Worm
DelfInject [20]	VirTool	Vundo [40]	Trojan Downloader
FakeRean [36]	Rogue	Winwebsec [41]	Rogue
Hotbar [1]	Adware	Zbot [23]	Password Stealer
Lolyda [21]	Password Stealer	Zegost [4]	Backdoor

Adload downloads an executable file, stores it remotely, executes the file, and disables proxy settings [29].

Agent downloads trojans or other software from a remote server [30].

Alureon exfiltrates usernames, passwords, credit card information, and other confidential data from an infected system [35].

BHO can perform a variety of actions, guided by an attacker [32].

CeeInject uses advanced obfuscation to avoid being detected by antivirus software [34].

Cycbot.G connects to a remote server, exploits vulnerabilities, and spreads through a backdoor [3].

DelfInject sends usernames, passwords, and other personal and private information to an attacker [20].

FakeRean pretends to scan the system, notifies the user of supposed issues, and asks the user to pay to clean the system [36].

Hotbar is adware that shows ads on webpages and installs additional adware [1].

Lolyda sends information from an infected system and monitors the system. It can share user credentials and network activity with an attacker [21].

Obfuscator tries to obfuscate or hide itself to defeat malware detectors [37].

Onlinegames steals login information and tracks user keystroke activity [22].

Rbot gives control to attackers via a backdoor that can be used to access information or launch attacks, and it serves as a gateway to infect additional sites [38].

Renos downloads software that claims the system has spyware and asks for a payment to remove the nonexistent spyware [31].

Startpage changes the default browser homepage and can perform other malicious activities [33].

Vobfus is a worm that downloads malware and spreads through USB drives or other removable drives [39].

Vundo displays pop-up ads and it can download files. It uses advanced techniques to defeat detection [40].

Winwebsec displays alerts that ask the user for money to fix nonexistent security issues [41].

Zbot is installed through email and shares a user’s personal information with attackers. In addition, Zbot can disable a firewall [23].

Zegost creates a backdoor on an infected machine [4].

The number of samples per malware family for the various features are given in Table 2. The “Binaries” lists the number of binary executable files available, the “Images” column lists the number of binaries that were successfully converted to images, and the “Opcodes” column lists the number of samples from which a sufficient number of opcodes were extracted. From the table we see that 26,413 samples are used in our image-based experiments and 25,901 samples are used in our opcode-based experiments.

Table 2: Samples per malware family

Family	Samples		
	Binaries	Images	Opcodes
Adload	1050	1050	1044
Agent	842	842	817
Alureon	1328	1328	1327
BHO	1176	1176	1159
CeeInject	894	894	886
Cycbot	1029	1029	1029
DelfInject	1146	1146	1097
Fakerean	1063	1063	1063
Hotbar	1491	1491	1476
Lolyda	915	915	915
Obfuscator	1445	1445	1331
Onlinegames	1293	1293	1284
Rbot	1017	1017	817
Renos	1312	1312	1309
Startpage	1136	1136	1084
Vobfus	926	926	924
Vundo	1793	1793	1784
Winwebsec	3651	3651	3651
Zbot	1786	1786	1785
Zeroaccess	1120	1120	1119
Total	26,413	26,413	25,901

2.4 Hardware

Table 3 lists the hardware configuration of the machine used for the experiments reported in this paper. This machine was assembled for the purpose of training deep learning models and it is highly optimized for this task.

2.5 Software

For our deep learning neural network experiments, we have used PyTorch [18]. In addition, for general data processing and related operations, we employ both Numpy [17] and Pandas [14]. In addition, all code that was developed as part of this project is available at [19].

3 Deep Learning Experiments and Results

In this section, we present results of a wide variety of neural network based experiments. First, we consider MLP experiments, followed by CNN experiments, and then RNN experiments. We consider a large number of CNN and RNN cases. We conclude this section with a pair of models based on transfer learning. The MLP, CNN, and transfer learning models are based on image features, while the RNN experiments use opcode sequences.

We consider various different sizes for images, in each case using square images. To generate a square image from an executable, we first specify a width N , with the height determined by the size of the sample. We then resize the image so that it is $N \times N$, which has the effect of stretching or shrinking the height, as required.

3.1 Multilayer Perceptron Experiments

We experimented with various perceptron-based neural networks. The model we present here uses square input image and has four hidden layers, each using the popular rectified linear unit (relu) activation function. The output from the final hidden layer is passed to a fully connected output layer. The output layer is used to classify the sample—since we have 20 classes of malware in our dataset, the output vector is 20-dimensional. The hyperparameters used for these MLP experiments are given in Table 4.

Figure 2 gives the confusion matrix for the best results obtained in our MLP experiments. The hyperparameters used for this best case are those shown in boldface in Table 4. In this case, the

Table 3: Hardware characteristics

Feature	Description	Details
CPU	Brand and model	Intel i9-9940X
	Clock Frequency	3.30GHz
	Number of threads	28
	Cache	19.25 MB Intel Smart Cache
CPU liquid cooling	Brand and model	Corsair Hydro Series H115i PRO RGB
	Fan Speed	1200 RPM
	Fan size	140mm
	Radiator size	280mm
DRAM	Brand and model	Corsair CMK32GX4M2A2666C16
	Speed	2666MHz
	Capacity	16 × 8 = 128GB
Motherboard	Brand and model	ASUS WS x299 Sage
GPU	Brand and model	Nvidia Titan RTX
	Total Video Memory	24 GB GDDR6
	Tensor Cores	576
	CUDA Cores	4608
	Base Clock (MHz)	1350 MHz
	Single-Precision Performance	16.3 TFLOPS
	Tensor Performance	130 TFLOPS
Storage	Brand and model	Sabrent 2TB Rocket NVMe
	Read Speed	3400 MB/s
	Write Speed	2750 MB/s

Table 4: MLP model parameters

Classifier	Hyperparameter	Tested values	Accuracy	
			Train	Test
MLP	image_dim	[64, 128]	0.9529	0.8644
	learning_rate	[0.001, 0.0001]		
	batch_size	256		
	epochs	50		

DelfInject and Obfuscator families have the lowest detection rates, with both only slightly above 50% accuracy. The overall accuracy is 0.8644.

3.2 Convolutional Neural Network Experiments

We have conducted a large number of convolutional neural network (CNN) experiments. In this section we first discuss CNN experiments based on 2-dimensional images. Then we consider 1-dimensional CNN experiments, where the malware images are vectorized. We also present results for CNN experiments using opcodes extracted from PE files, as opposed to forming images based on the raw byte values in the executable files. The opcodes were extracted using objdump, and we use the resulting mnemonic opcode sequence (eliminating operands, labels, etc.) as features. The hyperparameters tested for all of these CNN experiments are given in Table 5.

3.2.1 2-Dimensional Image CNNs

Based on 2-dimensional image features, we test the CNN model hyperparameters listed under “CNN 2-d” in Table 5. All of these 2-d CNN experiments use two convolutional layers and three fully connected layers. The first convolutional layer takes as input a square gray-scale image with one channel and outputs data with 12 channels using a kernel size of three, padding of two, and a stride of one. A relu activation and max pooling is applied to the result before passing it to the second

Table 5: CNN model parameters

Classifier	Hyperparameter	Tested values	Accuracy	
			Train	Test
CNN 2-d	image_dim	[64, 128, 256, 1024]	0.9294	0.8955
	learning_rate	[0.001 , 0.0001]		
	batch_size	256		
	epochs	50		
CNN 1-d	image_dim	[1024 , 2048, 4096, 8192]	0.8445	0.8664
	learning_rate	[0.001 , 0.0001]		
	batch_size	256		
	epochs	20		
CNN 1-d refined	conv1d_1_out_channel	[64, 128]	0.8538	0.8932
	conv1d_1_kernel_size	[16 , 32]		
	conv1d_1_stride	[2, 8]		
	conv1d_2_out_channel	[32 , 64, 128]		
	conv1d_2_kernel_size	[8 , 16]		
	conv1d_2_stride	[2 , 4]		
	image_dim	4096		
	learning_rate	0.001		
	batch_size	512		
	epochs	15		
CNN opcode	opcode_length	[500, 5000]	0.8418	0.8282
	num_filters	[3, 6, 9]		
	filter_size	[[12, 6], [6, 12], [12 , 24]]		
	embedding_dim	[128, 512]		
	learning_rate	0.001		
	batch_size	256		
	epochs	50		

convolutional layer. This second layer outputs data with 16 channels, with the other parameters being the same as the first convolutional layer. Again, relu activation and max pooling is applied before passing data to the first fully connected layer. This first fully connected layer outputs a vector of dimension 120. After applying relu activation, the data is passed to the second fully connected layer, which reduces the output to a 90 dimensional vector. Finally, relu activation is again applied and the data passes to the last fully connected layer, which is used to classify the sample, and hence is 20-dimensional. For all image sizes less than 1024, we execute our CNN 2-d models for 50 epochs; for 1024×1024 images, we use 8 epochs due to the costliness of training on these large images.

The best overall accuracy obtained for our CNN 2-d experiments is 0.8955. Figure 3 gives the confusion matrix for the best case. We note that the Obfuscator family is again the most difficult to distinguish.

3.2.2 Vectorized Image CNNs

Recent work has shown promising results for malware classification using 1-dimensional CNNs on “image” data [10]. Consequently, we experiment with flattened images, that is, we use images that are one pixel in height. A possible advantage of this approach is that 2-dimensional results can depend on the width chosen for the images. We perform two sets of such experiments, which we denote as CNN 1-d and CNN 1-d refined, the latter of which considers additional fine-tuning parameters. The hyperparameters tested for this two case are given in Table 5.

Our CNN 1-d model uses two 1-dimensional convolutional layers, followed by three fully connected layers. The first convolution layer takes in an image with one channel and outputs data with 28 channels based on a kernel size of three. The second convolutional layer outputs data with 16 channels and again uses a kernel of size three. The first fully connected layer outputs a vector of 120 dimensions, which is reduced to 90 dimensions by the second fully connected which, in turn, is reduced to 20 dimensions by the third (and last) fully connected layer. We have applied relu activations in all layers.

The confusion matrix for our best CNN 1-d case is give in Figure 4. The overall accuracy in in this case is 0.8664. A handful of families (Agnnet, Alureon, DelfInject, Obfuscator, and Rbot) have accuracies below 80%, which represents the majority of the loss of accuracy.

The CNN 1-d refined tests use the same basic setup as our CNN 1-d experiments, but includes different selections of hyperparameters. As expected, these additional parameters improved on the CNN 1-d case, as the best overall accuracy attained for our CNN 1-d refined experiments is 0.8932. Qualitatively, the CNN 1-d refined results are similar (per family) to the CNN 1-d experiments, so we have omitted the confusion matrix for this case.

3.2.3 Opcode Based CNNs

We also apply 2-d CNNs to opcode features. For each malware sample, we use the first N opcodes from each binary file, where $N \in \{500, 5000\}$. We also experiment with various other parameters, as indicated in Table 5.

The results for the best choice of parameters for our opcode-based CNN experiments are summarized in the confusion matrix in Figure 5. Perhaps not surprisingly, the results in this case are relatively weak, with an overall accuracy of 0.8282. However, it is interesting to note from the confusion matrix that some of the families that are consistently misclassified at high rates by image-based CNN models are classified with high accuracy by this opcode-based approach. For example, DelfInject is classified at no better than about 71% in our previous CNN experimetsn, but it is classified with greater than 90% accuracy using the opcode-based features.

3.3 Recurrent Neural Networks

Next, we consider a variety of experiments based on various recurrent neural network (RNN) architectures. Specifically, we employ plain vanilla RNN, LSTM, and GRU models. We also consider a complex LSTM-GRU stacked model. The hyperparameters tested in these experiments are summarized in Table 6.

3.3.1 Vanilla RNN, LSTM, and GRU

We have trained our plain vanilla RNNs, LSTMs, and GRU-based models using 20 epochs in each case, with a learning rate of 0.001, a batch size of 128, and based on the first 500 opcodes from each malware sample. We performed multiple experiments with various other parameters, as given in Table 6. In addition, we have applied a dropout layer with 0.3 probability for all models with more than one layer.

The vanilla RNN experiments performed poorly, with an overall accuracy of just 0.7294, and hence we omit the confusion matrix for this case. On the other hand, both the LSTM and GRU models perform well, with accuracies of 0.8916 and 0.9003, respectively. The confusion matrix for the GRU case is given in Figure 6. Since the LSTM results are so similar, we omit the LSTM confusion matrix. From Figure 6, we see that, qualitatively, the results of our GRU experiments more closely match those of the CNN opcode-based experiments than the CNN image-based experiments. However, quantitatively, our GRU opcode-based experiments yield significantly better results than our CNN opcode-based experiments.

3.3.2 Stacked LSTM-GRU Model

As in [7], we have also experimented with stacked LSTM and GRU layers. The experiments in this paper test more parameters and we use a larger dataset, as compared to [7]. A configuration option, which we refer to as LG, is used to decide whether the LSTM is stacked on top of the GRU (LG = false in this case) or GRU is stacked on top of the LSTM (LG = true). For example, when LG is “true,” opcode inputs are first passed to LSTM layers, with the output of the LSTM (i.e. the hidden cells) becoming input to the GRU layers. The output of the GRU is then passed to fully connected layers that are used to classify the input data. We have applied a dropout layer with 0.3 probability for models with more than one layer.

The best overall accuracy we obtain for our stacked LSTM-GRU experiments is 0.8990; the confusion matrix for this case is given in Figure 7. This is somewhat disappointing, as it is in between the results obtained for our LSTM and GRU models.

Table 6: RNN model parameters

Classifier	Hyperparameter	Tested values	Accuracy	
			Train	Test
RNN	embedding_dim	[256 , 1024]	0.7710	0.7294
	hidden_dim	[256 , 1024]		
	num_layers	[1, 3]		
	directional	[uni-dir, bi-dir]		
	learning_rate	0.001		
	batch_size	128		
	epochs	20		
LSTM	embedding_dim	[256 , 1024]	0.9362	0.8916
	hidden_dim	[256 , 1024]		
	num_layers	[1, 3]		
	directional	[uni-dir, bi-dir]		
	learning_rate	0.001		
	batch_size	128		
	epochs	20		
GRU	embedding_dim	[256 , 1024]	0.9411	0.9003
	hidden_dim	[256 , 1024]		
	num_layers	[1, 3]		
	directional	[uni-dir, bi-dir]		
	learning_rate	0.001		
	batch_size	128		
	epochs	20		
Stacked	embedding_dim	[256, 1024]	0.9525	0.8990
	hidden_dim	[256, 1024]		
	num_layers	[1, 3]		
	directional	[uni-dir, bi-dir]		
	LG	[True, False]		
	learning_rate	0.001		
	batch_size	128		
epochs	20			

3.4 Transfer Learning

Finally, we have considered two popular image-based transfer learning models, namely ResNet152 and VGG-19. These are models that have been pre-trained on extremely large image datasets, and we simply retrain the last few layers for the malware dataset under consideration in this paper, while the earlier layers are frozen during training. The parameters used in these experiments are summarized in Table 7.

Table 7: Transfer learning model parameters

Classifier	Hyperparameter	Tested values	Accuracy	
			Train	Test
ResNet152	image_dim	256	0.9811	0.9150
	learning_rate	[0.001, 0.0001]		
	batch_size	256		
	epochs	20		
VGG-19	image_dim	256	0.9690	0.9216
	learning_rate	[0.001, 0.0001]		
	batch_size	256		
	epochs	20		

For ResNet152, the model parameters for layer four were unfrozen for training. We also added two more layers of fully connected neurons for training. Resnet152 is pre-trained based on 1000 classes and hence its last fully connected layer has output dimensions of 1000. We reduce this output dimension to 500 via another fully connected layer, and an additional fully connected layer further reduces the output dimension to 20, which is the number of classes in our dataset.

For VGG-19, we froze all layers except 34, 35, and 36. As with ResNet152, we added two more layers of fully connected neurons to reduce the output dimension from 1000 to 20.

For all of our transfer learning experiments, we use a batch size of 256 and trained each model for 20 epochs with learning rates of 0.001 and 0.0001. Both ResNet152 and VGG-19 expect image dimensions of 224×224 and hence we resize our 256×256 images to 224×224 .

The performance of these transfer learning models was the best of our deep learning experiments, with ResNet152 achieving an overall accuracy of 0.9150 and VGG-19 doing slightly better at 0.9216. The confusion matrix for VGG-19 is given in Figure 8; we omit the confusion matrix for ResNet152 since it is similar, but marginally worse. As compared to the other image-based deep learning models we have considered, we see marked improvement in the classification accuracy of the most challenging families, such as Obfuscator.

3.5 Discussion

The results of the malware classification experiments discussed in this section are summarized in Figure 1. We see that among the deep learning techniques, the image-based pre-trained models, namely, ResNet152 and VGG-19, perform best, with VGG-19 classifying more than 92% of the samples correctly. The best of our other (i.e., not pre-trained) image-based models achieved slightly less than 90% accuracy.

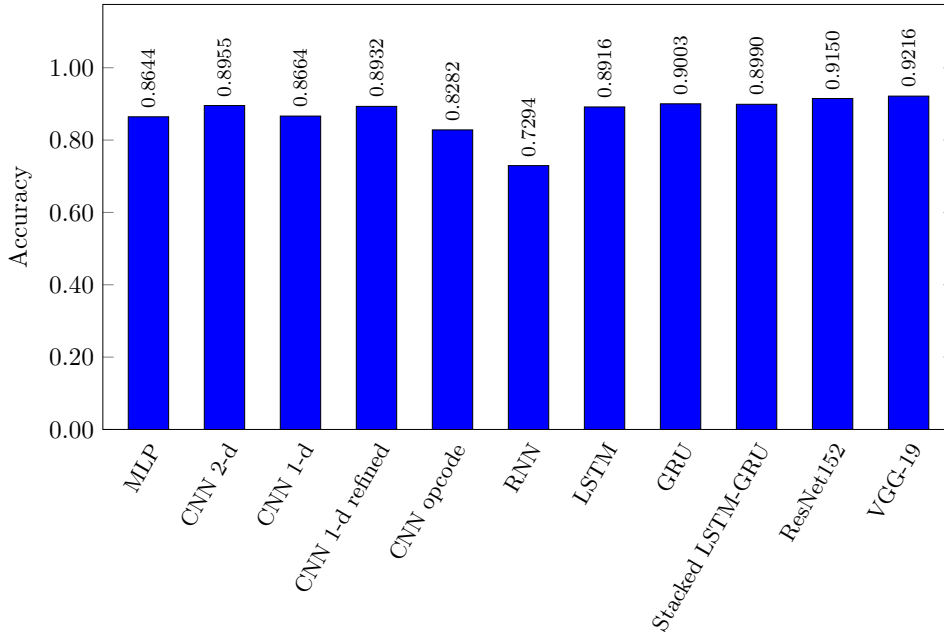


Figure 1: Comparison of results

Although the opcode-based results performed relatively poorly overall, it is interesting to note that they were able to classify some families with higher accuracy than any of the image-based models. This suggests that a model that combines both image features and opcode features might be more effective than either approach individually.

4 Conclusions and Future Work

Malware classification is a fundamental and challenging problem in information security. Previous work has indicated that treating malware executables as images and applying image-based techniques can yield strong classification results.

In this paper, we provided results from a vast number of learning experiments, comparing deep learning techniques using image-based features to some cases involving opcode features. For our deep learning techniques, we focused on multilayer perceptrons (MLP), convolutional neural networks (CNN), and recurrent neural networks (RNN), including long short-term memory (LSTM) and gated recurrent units (GRU). We also experimented with the image-based transfer learning techniques ResNet152 and VGG-19. Among these techniques, the image-based transfer learning models performed the best, with the best classification accuracy exceeding 92%.

For future work, additional transfer learning experiments would be worthwhile, as there are many more parameters that could be tested. Larger and more diverse datasets could be considered. In addition, it would be interesting to consider both image-based and opcode features as part of a combined classification technique. As noted above, the opcode-based techniques perform worse overall, but they do provide better results for some families that are particularly challenging to distinguish based only on image features.

References

- [1] Adware:win32/hotbar. [https://www.microsoft.com/en-us/wdsi/threats/malware-encyclopedia-description?Name=](https://www.microsoft.com/en-us/wdsi/threats/malware-encyclopedia-description?Name=Adware:win32/hotbar)
- [2] Thomas H. Austin, Eric Filiol, Sébastien Josse, and Mark Stamp. Exploring hidden Markov models for virus analysis: A semantic approach. In *46th Hawaii International Conference on System Sciences, HICSS 2013, Wailea, HI, USA, January 7-10, 2013*, pages 5039–5048. IEEE Computer Society, 2013.
- [3] Backdoor:win32/cycbot.g. [https://www.microsoft.com/en-us/wdsi/threats/malware-encyclopedia-description?Name=](https://www.microsoft.com/en-us/wdsi/threats/malware-encyclopedia-description?Name=Backdoor:win32/cycbot.g)
- [4] Backdoor:win32/zegost.ad. [https://www.microsoft.com/en-us/wdsi/threats/malware-encyclopedia-description?Name=](https://www.microsoft.com/en-us/wdsi/threats/malware-encyclopedia-description?Name=Backdoor:win32/zegost.ad)
- [5] Donabelle Baysa, Richard M. Low, and Mark Stamp. Structural entropy and metamorphic malware. *Journal of Computer Virology and Hacking Techniques*, 9(4):179–192, 2013.
- [6] Niket Bhodia, Pratikumar Prajapati, Fabio Di Troia, and Mark Stamp. Transfer learning for image-based malware classification. <https://arxiv.org/abs/1903.11551>, 2019.
- [7] Ero Carrera. pefile 2019.4.18. <https://pypi.org/project/pefile/>, 2019.
- [8] Anusha Damodaran, Fabio Di Troia, Corrado Aaron Visaggio, Thomas H. Austin, and Mark Stamp. A comparison of static, dynamic, and hybrid analysis for malware detection. *Journal of Computer Virology and Hacking Techniques*, 13(1):1–12, 2017.
- [9] Arpit Gupta. Alexa blogs: How Alexa is learning to converse more naturally. [https://developer.amazon.com/blogs/alexa/post/15bf7d2a-5e5c-4d43-90ae-c2596c9cc3a6/how-alexa-is-learning](https://developer.amazon.com/blogs/alexa/post/15bf7d2a-5e5c-4d43-90ae-c2596c9cc3a6/how-alexa-is-learning-to-converse-more-naturally) 2018.
- [10] Mugdha Jain, William Andreopoulos, and Mark Stamp. Convolutional neural networks and extreme learning machines for malware classification. *Journal of Computer Virology and Hacking Techniques*, 2020. To appear.
- [11] Pranav Khaitan. Google AI blog: Chat smarter with Allo. <https://ai.googleblog.com/2016/05/chat-smarter-with-allo.html>, 2016.
- [12] Samuel Kim. PE header analysis for malware detection. Master’s thesis, San Jose State University, 2018. https://scholarworks.sjsu.edu/etd_projects/624/.
- [13] Steven Levy. The iBrain is here—and it’s already inside your phone. *Wired*. <https://www.wired.com/2016/08/an-exclusive-look-at-how-ai-and-machine-learning-work-at-apple/>, 2016.
- [14] Wes McKinney. Pandas 1.0.5: Powerful data structures for data analysis, time series, and statistics. <https://pypi.org/project/pandas/>, 2020.
- [15] Antonio Nappa, M Zubair Rafique, and Juan Caballero. The malicia dataset: identification and analysis of drive-by download operations. *International Journal of Information Security*, 14(1):15–33, 2015.
- [16] L. Nataraj, S. Karthikeyan, G. Jacob, and B. S. Manjunath. Malware images: Visualization and automatic classification. In *Proceedings of the 8th International Symposium on Visualization for Cyber Security, VizSec ’11*, 2011.
- [17] Travis Oliphant. NumPy: A guide to NumPy. <http://www.numpy.org/>, 2006.
- [18] Adam Paszke, Sam Gross, Soumith Chintala, and Gregory Chanan. PyTorch: From research to production. <https://pytorch.org/>, 2016.

- [19] Pratikumar Prajapati. Github repository. https://github.com/pratikpv/malware_detect2, 2020.
- [20] Pws:win32/delfinject. <https://www.microsoft.com/en-us/wdsi/threats/malware-encyclopedia-description?Name=PWS:Win32/Delfinject>.
- [21] Pws:win32/lolyda.bf. <https://www.microsoft.com/en-us/wdsi/threats/malware-encyclopedia-description?Name=PWS:Win32/Lolyda.bf>.
- [22] Pws:win32/onlinegames. <https://www.microsoft.com/en-us/wdsi/threats/malware-encyclopedia-description?Name=PWS:Win32/OnlineGames>.
- [23] Pws:win32/zbot. <https://www.microsoft.com/en-us/wdsi/threats/malware-encyclopedia-description?Name=PWS:Win32/Zbot>.
- [24] Karen Simonyan and Andrew Zisserman. Very deep convolutional networks for large-scale image recognition. <https://arxiv.org/abs/1409.1556>, 2014.
- [25] Tanuvir Singh, Fabio Di Troia, Corrado Aaron Visaggio, Thomas H. Austin, and Mark Stamp. Support vector machines and malware detection. *Journal of Computer Virology and Hacking Techniques*, 12(4):203–212, 2016.
- [26] Nelson Spruston. Pyramidal neurons: Dendritic structure and synaptic integration. *Nature Reviews Neuroscience*, 9:206–221, 2019. <https://www.nature.com/articles/nrn2286>.
- [27] Mark Stamp. A selective survey of deep learning techniques and their application to malware analysis. In Mark Stamp, Mamoun Alazab, and Andrii Shalaginov, editors, *Malware Analysis using Artificial Intelligence and Deep Learning*, chapter 1, pages 1–48. Springer, 2020.
- [28] Annie H. Toderici and Mark Stamp. Chi-squared distance and metamorphic virus detection. *Journal of Computer Virology and Hacking Techniques*, 9(1):1–14, 2013.
- [29] Trojandownloader:win32/adload. <https://www.microsoft.com/en-us/wdsi/threats/malware-encyclopedia-description?Name=Trojandownloader:Win32/Adload>.
- [30] Trojandownloader:win32/agent. <https://www.microsoft.com/en-us/wdsi/threats/malware-encyclopedia-description?Name=Trojandownloader:Win32/Agent>.
- [31] Trojandownloader:win32/renos. <https://www.microsoft.com/en-us/wdsi/threats/malware-encyclopedia-description?Name=Trojandownloader:Win32/Renos>.
- [32] Trojan:win32/bho. <https://www.microsoft.com/en-us/wdsi/threats/malware-encyclopedia-description?Name=Trojan:Win32/BHO>.
- [33] Trojan:win32/startpage. <https://www.microsoft.com/en-us/wdsi/threats/malware-encyclopedia-description?Name=Trojan:Win32/Startpage>.
- [34] Virtool:win32/ceeinject. <https://www.microsoft.com/en-us/wdsi/threats/malware-encyclopedia-description?Name=Virtool:Win32/Ceeinject>.
- [35] Win32/alureon. <https://www.microsoft.com/en-us/wdsi/threats/malware-encyclopedia-description?Name=Win32/Alureon>.
- [36] Win32/fakerean. <https://www.microsoft.com/en-us/wdsi/threats/malware-encyclopedia-description?Name=Win32/Fakerean>.
- [37] Win32/obfuscator. <https://www.microsoft.com/en-us/wdsi/threats/malware-encyclopedia-description?Name=Win32/Obfuscator>.
- [38] Win32/rbot. <https://www.microsoft.com/en-us/wdsi/threats/malware-encyclopedia-description?Name=Win32/Rbot>.
- [39] Win32/vobfus. <https://www.microsoft.com/en-us/wdsi/threats/malware-encyclopedia-description?Name=Win32/Vobfus>.
- [40] Win32/vundo. <https://www.microsoft.com/en-us/wdsi/threats/malware-encyclopedia-description?Name=Win32/Vundo>.
- [41] Win32/winwebsec. <https://www.microsoft.com/en-us/wdsi/threats/malware-encyclopedia-description?Name=Win32/Winwebsec>.
- [42] Wing Wong and Mark Stamp. Hunting for metamorphic engines. *Journal in Computer Virology*, 2(3):211–229, 2006.
- [43] Yonghui Wu, Mike Schuster, Zhifeng Chen, Quoc V. Le, Mohammad Norouzi, Wolfgang Macherey, Maxim Krikun, Yuan Cao, Qin Gao, Klaus Macherey, Jeff Klingner, Apurva Shah, Melvin Johnson, Xiaobing Liu, Łukasz Kaiser, Stephan Gouws, Yoshikiyo Kato, Taku Kudo, Hideto Kazawa, Keith Stevens, George Kurian, Nishant Patil, Wei Wang, Cliff Young, Jason Smith, Jason Riesa, Alex Rudnick, Oriol Vinyals, Greg Corrado, Macduff Hughes, and Jeffrey Dean. Google’s neural machine translation system: Bridging the gap between human and machine translation. <https://arxiv.org/abs/1609.08144>, 2016.
- [44] S. Yajamanam, V. R. S. Selvin, F. Di Troia, and Mark Stamp. Deep learning versus gist descriptors for image-based malware classification. In *Proceedings of the 4th International Conference on Information Systems Security and Privacy, ICISSP 2018*, pages 553–561, 2018.

Appendix: Confusion Matrices

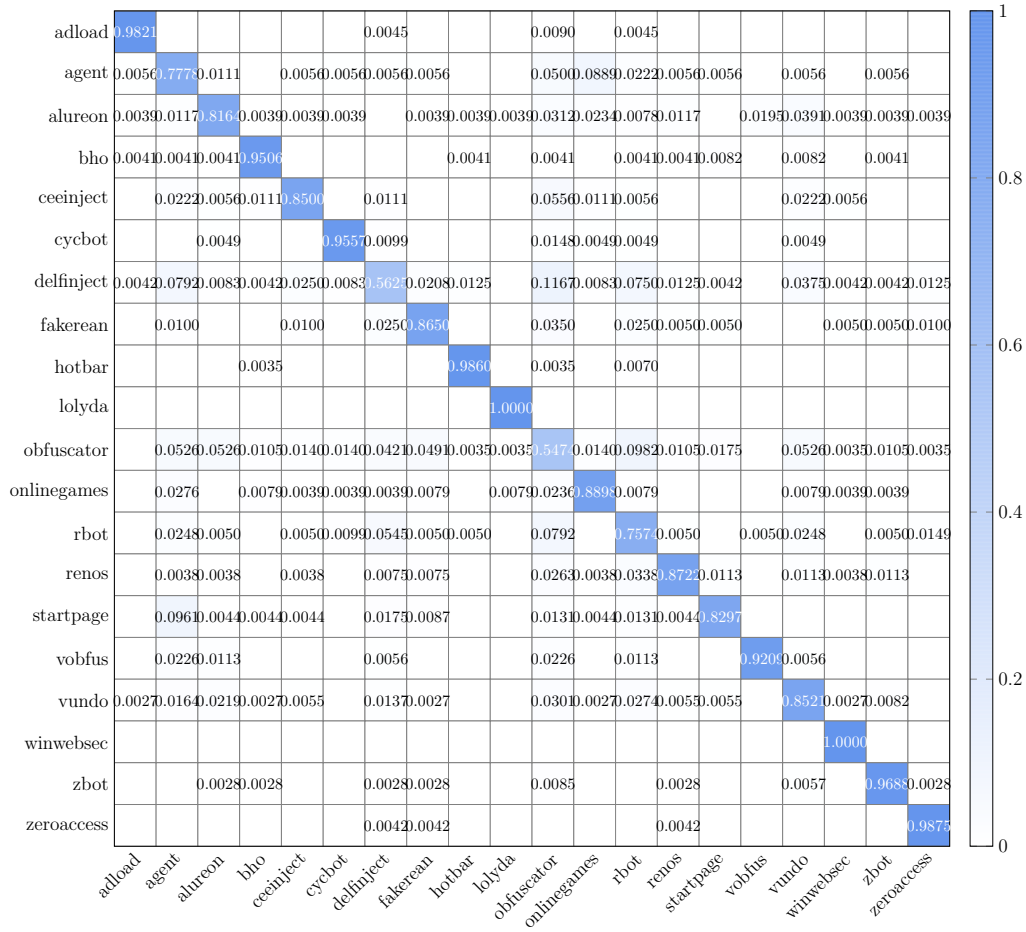


Figure 2: Confusion matrix for MLP experiment

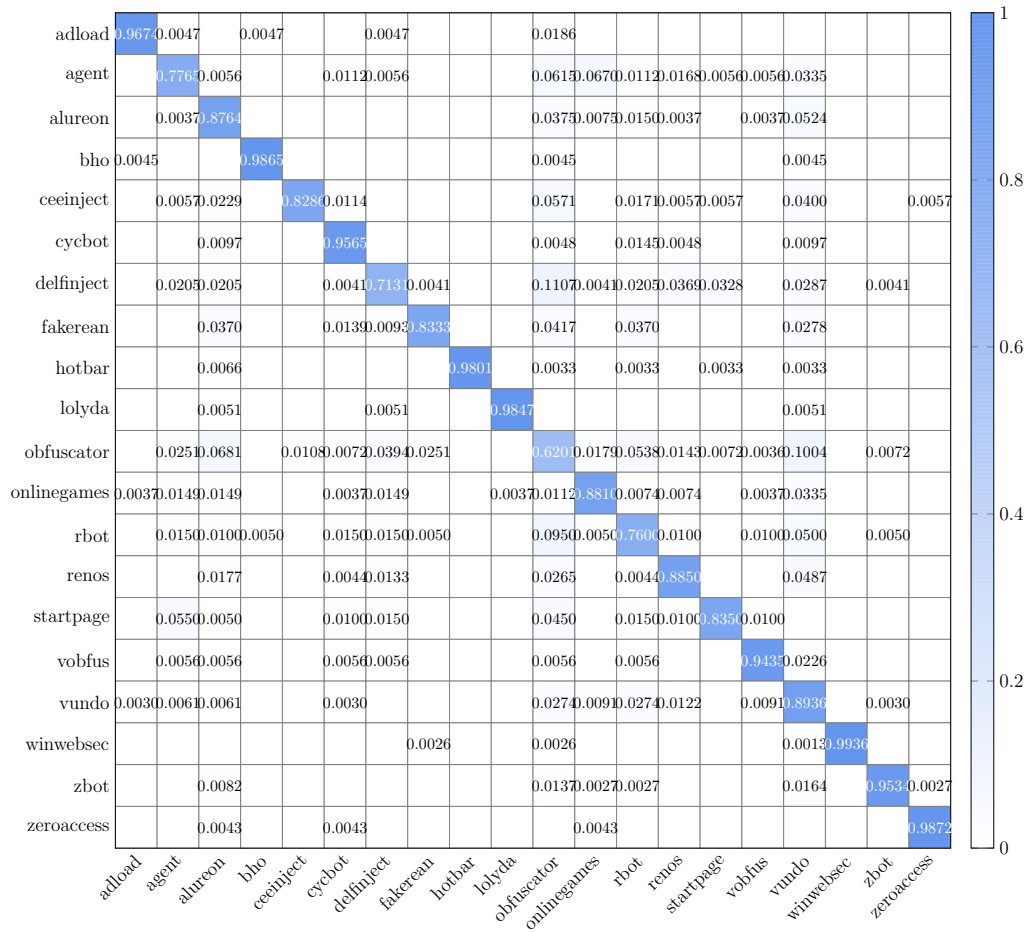


Figure 3: Confusion matrix for CNN 2-d experiment

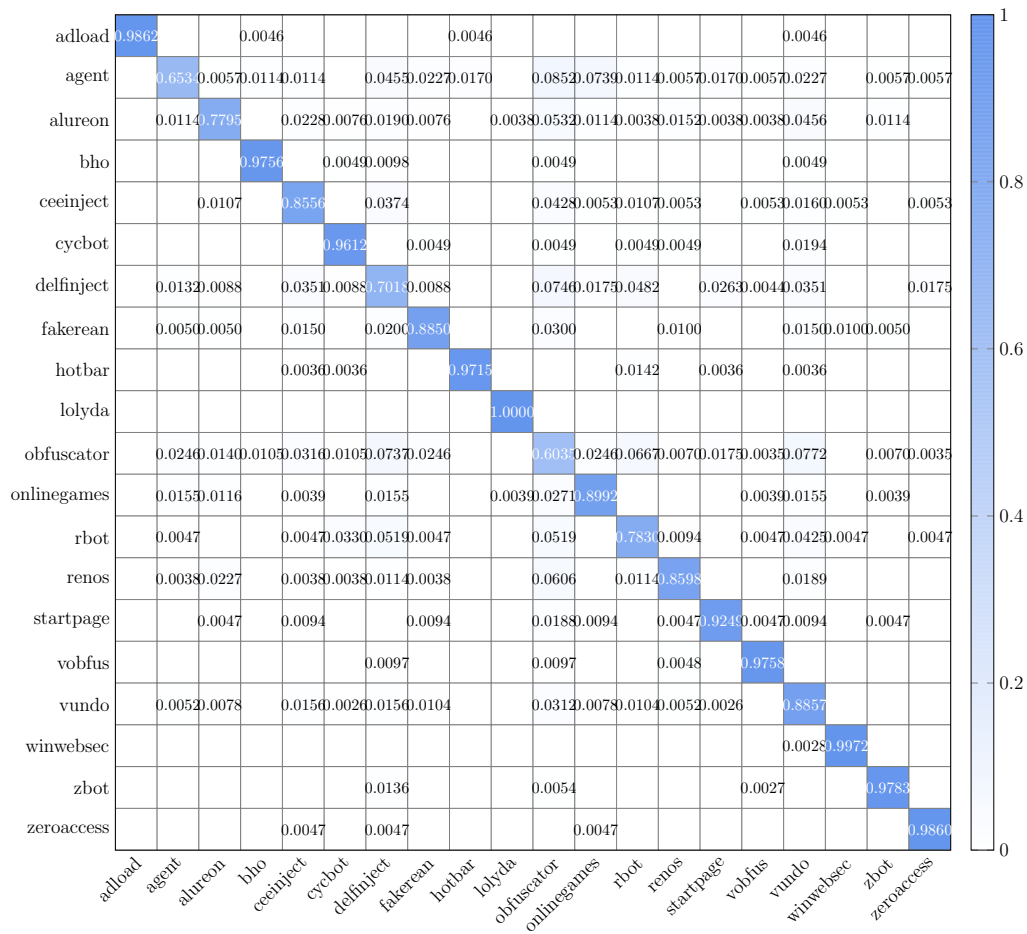


Figure 4: Confusion matrix for CNN 1-d experiment

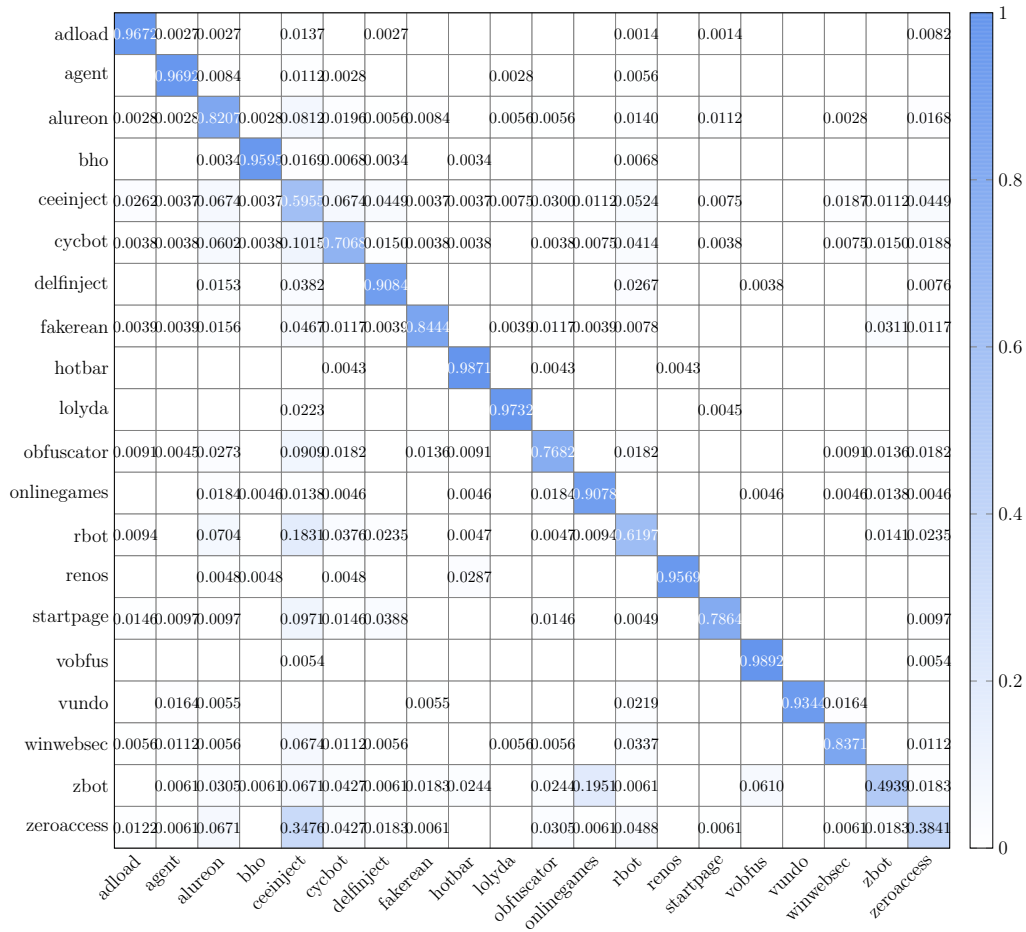


Figure 5: Confusion matrix for opcode-based CNN experiment

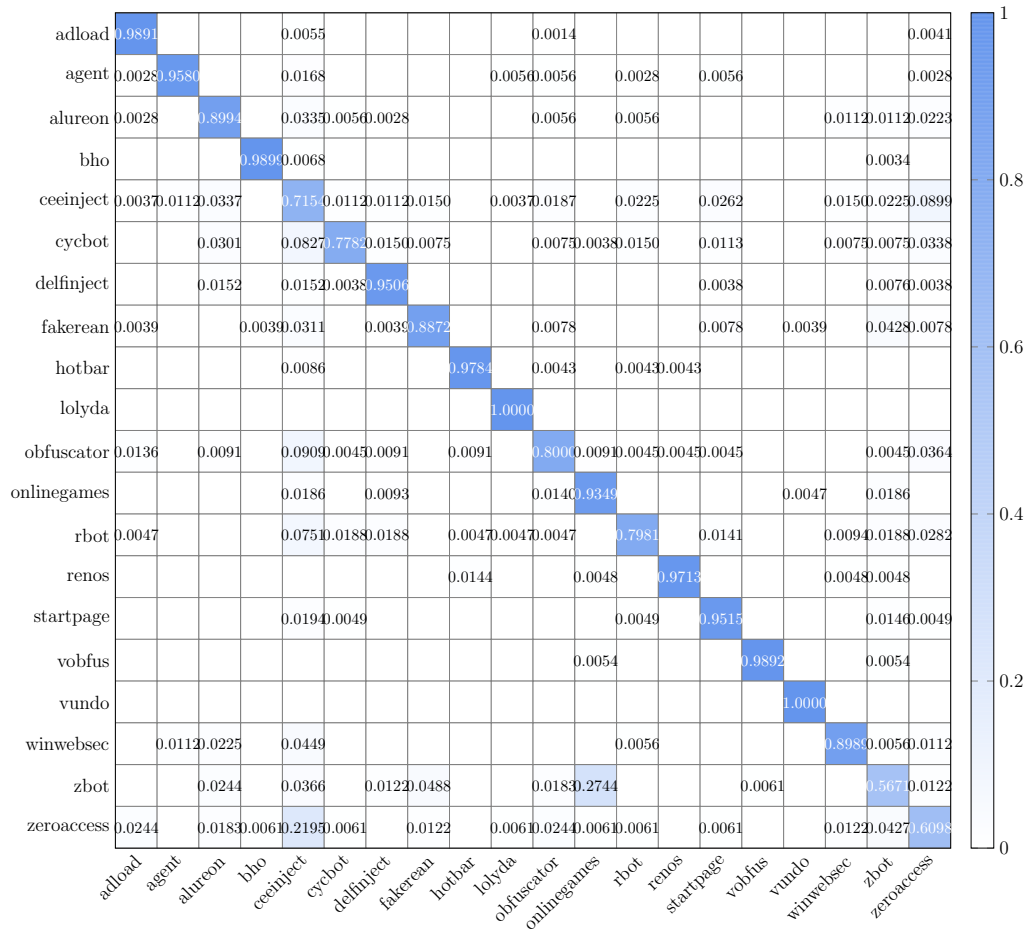


Figure 6: Confusion matrix for GRU experiment

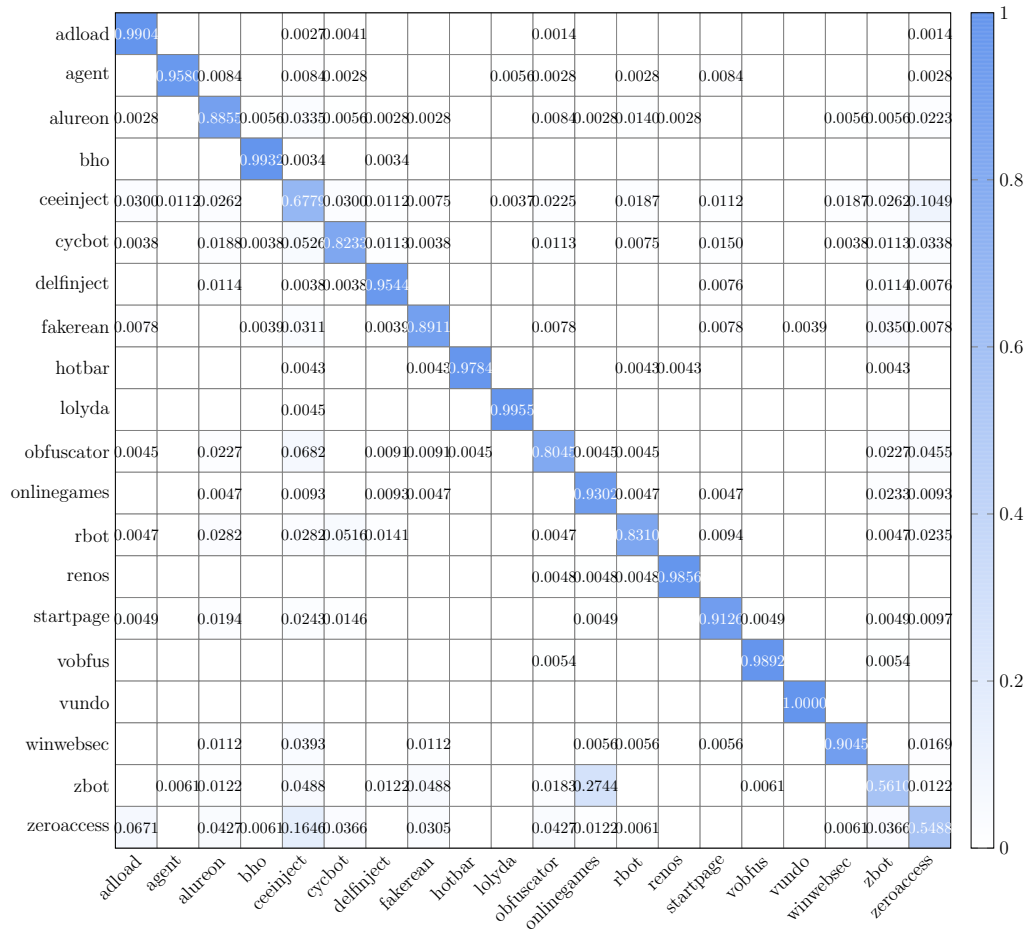


Figure 7: Confusion matrix for stacked LSTM-GRU experiment

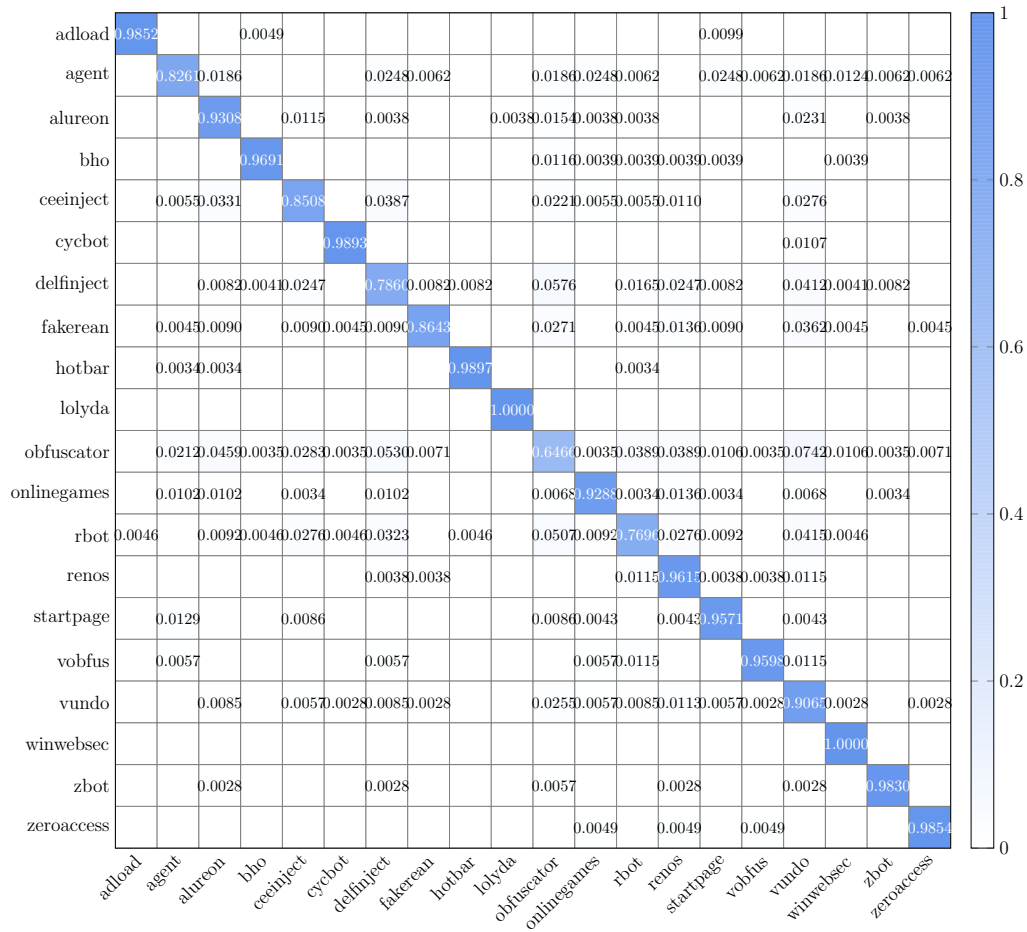


Figure 8: Confusion matrix for VGG-19 experiment